Chemical Science

ROYAL SOCIETY OF CHEMISTRY

EDGE ARTICLE

View Article Online
View Journal | View Issue



Cite this: *Chem. Sci.*, 2020, **11**, 1935

All publication charges for this article have been paid for by the Royal Society of Chemistry

Received 20th November 2019
Accepted 8th January 2020

DOI: 10.1039/c9sc05881h

rsc.li/chemical-science

# Auto-controlled fabrication of a metal-porphyrin framework thin film with tunable optical limiting effects†

De-Jing Li, [ab] Zhi-Gang Gu *[a] and Jian Zhang *[a]

Metal–organic frameworks (MOFs) with third-order nonlinear optical (NLO) properties are still in their infancy but are very important. In this work, we first develop a layer by layer autoarm immersion method for preparing porphyrin-based MOF (PIZA-1) thin films with third-order NLO properties. By precisely controlling the thickness, the nonlinear absorption of PIZA-1 thin films can be switched continuously between reverse saturable absorption (RSA) and saturable absorption (SA) by using the Z-scan technique. In addition, the optical limiting effect could be further optimized by loading $C_{60}$ in the pores of the PIZA-1 thin film. These findings not only open a new route for the exploitation of third-order NLO thin film materials, but also offer an insightful understanding of porphyrin-based MOF thin films for future broad practical applications.

## Introduction

Third-order nonlinear optical (NLO) materials have attracted much attention due to their potential applications in optical switching, optical limiting, logic devices, image transmission and mode-locked laser systems.[1–5] Thus, the design and synthesis of new third-order NLO materials are important in modern chemistry and materials science. The NLO behavior mainly includes reverse saturable absorption (RSA), saturable absorption (SA), nonlinear scattering (NLS), nonlinear refraction (NLR), *etc.* So far, various organic/inorganic and hybrid materials have been synthesized for third-order NLO response, including carbon nanodots, semiconductor quantum dots, conjugated organic molecules (porphyrins and phthalocyanines) or polymers, black phosphorus, metal-oxo clusters and so on.[6–11] As a kind of porous crystalline hybrid material, metal–organic frameworks (MOFs)[12–15] are constructed by the coordination of metal nodes (clusters) with organic linkers and are supposed to be promising candidates to exploit optical properties including NLO behaviour, upconversion luminescence, lasing and so on.[16–20] A few cases of powder MOFs have been realized to investigate the third-order NLO properties.[21–23] However, such powder MOFs have large scattering and are usually required to be dispersed in solvents for investigating the third-order NLO properties. Thus it is difficult to avoid the influence from solvents. So far, MOFs in the form of thin films have not been studied in terms of their third-order NLO properties, but they are important for practical applications.

Recently, MOF thin films have been used in various applications.[24–28] In particular, the liquid-phase epitaxy (LPE) layer by layer method has been widely used for preparation of MOF thin films on substrate surfaces (also called SURMOFs)[29–32] which showed controllable thickness, a homogeneous surface, compactness, controllable growth orientation and effective loading of functional guests into MOF pores.[33–36] Such high-quality MOF thin films will offer an opportunity for tuning the third-order NLO performance and enhancing practical device applications, such as pulse compression, Q-switching, mode-locking and optical limiting. In addition, as a special subclass of MOFs, metal-porphyrin frameworks (also called porphyrin-based MOFs) have interesting properties for catalysis, conductivity and photo-electric effects.[37–41] Moreover, highly π-conjugated porphyrin based materials are well-known to exhibit good third-order NLO response, particularly the optical limiting effect.[42,43] Therefore, the porphyrin-based MOF thin films may be promising materials for third-order NLO response, but no reports are available so far.

Herein, we develop a universal layer by layer autoarm immersion method with heating for the preparation of MOF thin films. This method is very labor-saving and cost-effective and can be widely applied to prepare MOF thin films (such as many classic MOFs HKUST-1, MOF-2, $Co_2(BDC)_2TED$, PIZA-1, *etc*). The autoarm immersion setup and preparation process of MOFs and guest loaded MOF thin films are shown in Fig. S1.† Notably, as a porphyrin-based MOF, the high quality PIZA-1 thin film is an ideal candidate for studying the third-order NLO properties. Here we first prepare the porphyrin-based MOF

[a]State Key Laboratory of Structural Chemistry, Fujian Institute of Research on the Structure of Matter, Chinese Academy of Sciences, Fuzhou, Fujian 350002, P. R. China. E-mail: zggu@fjirsm.ac.cn; zhj@fjirsm.ac.cn

[b]University of Chinese Academy of Sciences, Beijing 100049, P. R. China

† Electronic supplementary information (ESI) available. See DOI: 10.1039/c9sc05881h

PIZA-1 thin film on quartz glass by tuning the thickness and loading fullerene molecules in the pores of the PIZA-1 thin film (Fig. 1). Such a PIZA-1 thin film with different thicknesses showed switching of the nonlinear absorption from reverse saturable absorption (RSA) to saturable absorption (SA) and the optical limiting effect could be further improved by loading $C_{60}$ molecules. The superior optical limiting effect of the $C_{60}$ loaded PIZA-1 thin film may be attributed to the accumulation effect of energy transfer/photoinduced electron transfer (ET/PET) between the porphyrin group and $C_{60}$, RSA, nonlinear scattering (NLS), and nonlinear refraction (NLR). Density functional theory (DFT) calculations reveal that the ET/PET derived from electron-donor/electron–acceptor interactions can enhance the RSA behavior, which will optimize the optical limiting effect.

## Results and discussion

Fig. 2a and b show the structure and X-ray diffraction pattern of the PIZA-1 thin film, respectively. Two obvious XRD peaks of the PIZA-1 thin film located at 6.1 and 12.2 were observed, indicating a [110]-oriented thin film.[44] To study the thickness-dependent NLO behavior, PIZA-1 thin films prepared with 5, 10, 15, 20, and 25 cycles were grown on quartz glass under the same conditions. The SEM image (Fig. 2c) of the PIZA-1 thin film showed a homogeneous surface and a continuous thin film as well as an average domain width size of 1.4 μm (Fig. S2a†). Moreover, the PIZA-1 thin film has a low surface roughness of ~10 nm (Fig. S2b†), and the thicknesses of the PIZA-1 thin films (Fig. S2c†) are ~130, ~230, ~300, ~360 and ~420 nm for 5, 10, 15, 20 and 25 cycles (named PIZA-1-*n*, *n* is the LPE cycle number), showing an approximately linear dependence on the LPE cycles (Fig. 2d). This illustrates that the PIZA-1 thin film can be prepared successfully and the thickness can be well controlled by the layer by layer process. In addition, the transmittance of the PIZA-1 thin film with different thicknesses decreases with the increasing thickness (Fig. 2e and f) showing an approximate exponential decay with LPE cycles, and the absorbance of the PIZA-1 thin film prepared with different cycles exhibits an approximate exponential increase with LPE cycles. After fitting the data, the points were identical to the fitted nonlinear curve according to the equation $A = 2 - \log(T)$. In order to show the universality of the thin film preparation method, MOFs HKUST-1, MOF-2 and $Co_2(BDC)_2TED$ thin films are successfully prepared in this work, which can be demonstrated by the XRD and SEM characterization data in Fig. S3–S5.†

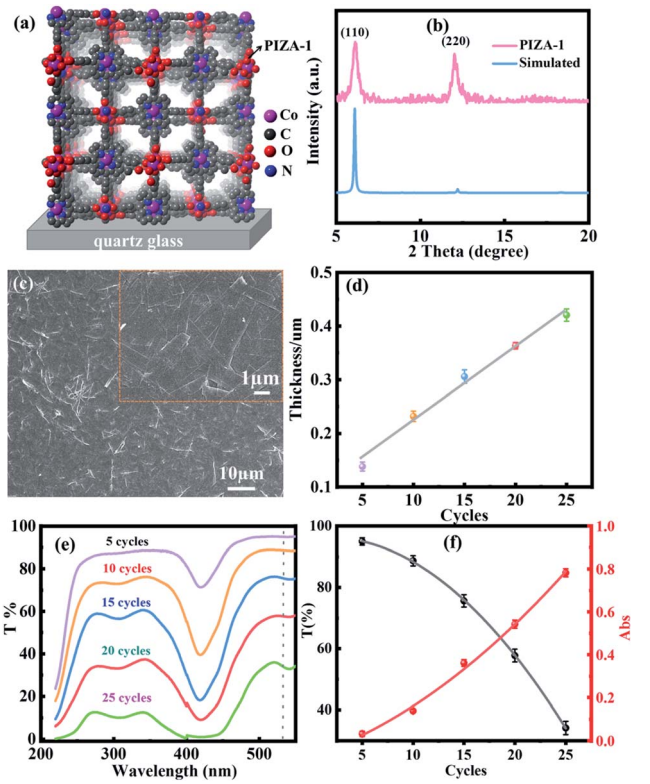


Fig. 2 (a) Structure of the PIZA-1 thin film; (b) XRD pattern of the PIZA-1 thin film; (c) surface SEM image of the PIZA-1 thin film prepared with 10 cycles; (d) plot of the thickness *versus* preparation cycles; (e) transmittance curves of the PIZA-1 thin film prepared with different cycles; (f) curves of the transmittance and absorbance *versus* preparation cycles.

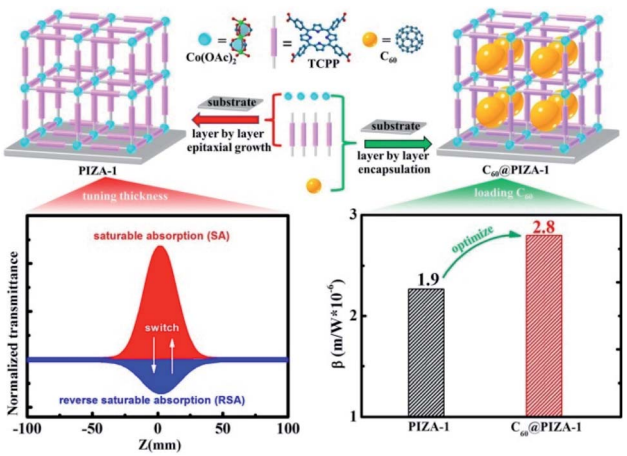


Fig. 1 The preparation of PIZA-1 and $C_{60}$@PIZA-thin films by the autoarm immersion layer by layer method and tunable NLO behavior by tuning the thickness and loading of fullerene molecules.

The NLO properties of the PIZA-1 thin film with different thicknesses grown on quartz glass (Fig. 3b) are studied using a typical open and closed aperture Z-scan system (Fig. 3a) with a nanosecond laser at 532 nm. As shown in Fig. 3c–g, PIZA-1-5 and PIZA-1-10 thin films exhibit a typical RSA response and the RSA response increases with the increase of the incident pulse energy. The minimum normalized transmittances ($T_{min}$) at $Z = 0$ are about 1 (30 μJ), 0.96 (50 μJ), 0.81 (80 μJ) and 0.74 (100 μJ) for PIZA-1-5 and 0.87 (30 μJ), 0.78 (50 μJ), 0.70 (30 μJ) and 0.65 (100 μJ) for PIZA-1-10, suggesting that PIZA-1-5 and PIZA-1-10 have a good RSA response with an optical limiting effect at 532 nm. PIZA-1-15 and PIZA-1-20 thin films show RSA responses at low pulse energy (30 and 50 μJ) first and then display a switching behavior from RSA to SA response after ~80 μJ. The normalized transmittance of PIZA-1-25 gradually

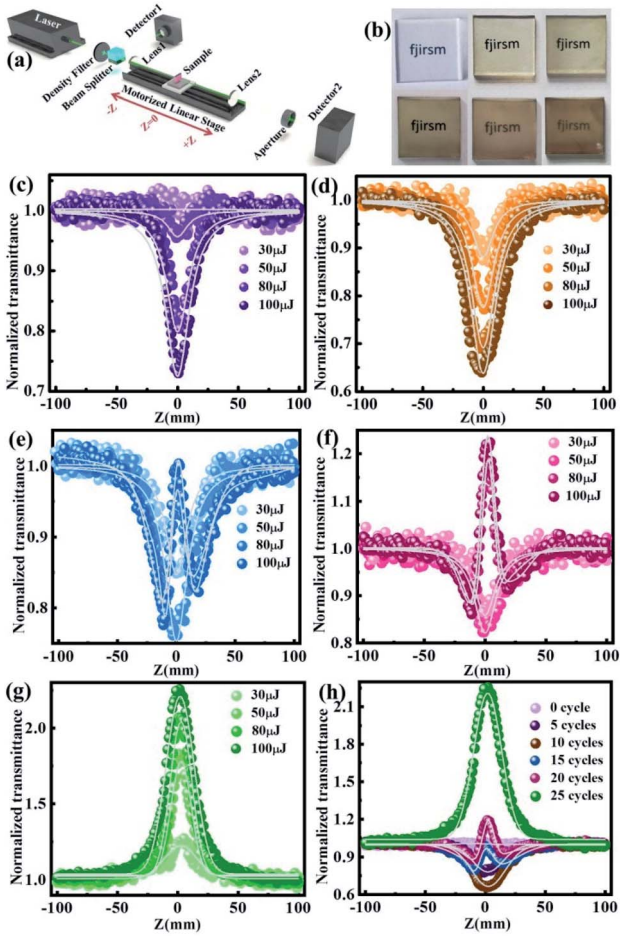


Fig. 3 (a) A typical open and closed aperture Z-scan system; (b) photograph of the PIZA-1 thin films on quartz glass with different thicknesses; third-order NLO behavior of the PIZA-1 thin films with different thicknesses: (c–g) 5, 10, 15, 20 and 25 cycles; (h) the thickness-dependent NLO behavior of the PIZA-1 thin films at an incident pulse energy of 100 μJ.

increases and this SA behavior could allow it to be developed as a passive mode locker or Q-switcher for ultrafast laser pulse generation.

The nonlinear absorption coefficient $\beta$ was calculated by fitting the Z-scan curves from Fig. 3c, d, and g and is shown in Table S1 and Fig. S6.† The negative value represents the SA response while the positive value corresponds to the RSA response.[45] The increase of $\beta$ with incident pulse energy implies that the nonlinear absorption is also influenced by nonlinear scattering in the high-fluence regime.[46] To compare the NLO behavior of the PIZA-1 thin film with different thicknesses clearly, a comparison of the results obtained at the same incident pulse energy of 100 μJ is shown in Fig. 3h and S7, S8.† The switching from RSA to SA with the increasing thickness was clearly observed. For the PIZA-1-15 and PIZA-1-20, the RSA-SA-RSA switching behavior can be attributed to the dominant excited state absorption at lower intensities (far from the laser focus) and saturation of excited states at higher intensity (near the laser focus).[47] Furthermore, the UV-vis absorbance spectra (Fig. S9†) showed that the absorbance of the PIZA-1 thin film increased with the increasing thickness. The band gaps of the PIZA-1 thin films with different thicknesses (Fig. S10†) were calculated to be the same, ~1.73 eV. Therefore, the thickness dependence of the NLO behavior can be attributed to the transmittance decrease of the PIZA-1 thin films with the increasing thickness. The behavior resulted in the nonlinear absorption of the PIZA-1 thin film changing from RSA to SA when tuning the thickness.

Another effective approach for tuning the NLO response is introducing guest species into MOF thin films. Herein an effective method of enhancing the NLO properties is introducing $C_{60}$ into the thin film due to its good RSA behavior. The $C_{60}$ loaded PIZA-1 ($C_{60}$@PIZA-1) thin film prepared with 10 cycles on quartz glass was prepared successfully by the modified autoarm immersion layer by layer approach. The successful loading of $C_{60}$ in the PIZA-1 thin film was proved by the characterization results such as the quartz crystal microbalance (QCM) results (Fig. S11†), UV-vis absorption spectrum (Fig. S12†), photocurrent response (Fig. S13†) and current–voltage curves (Fig. S14†). For comparison, all experiments were carried out with the same treatment. The water uptakes of PIZA-1 and $C_{60}$@PIZA-1 thin films in the QCM test were calculated to be 4.94 mg $cm^{-2}$ and 1.91 mg $cm^{-2}$, demonstrating that $C_{60}$ molecules were loaded in the pores successfully. Absorption bands at 330 nm were observed in the UV-vis absorption spectrum of the $C_{60}$@PIZA-1 thin film and the enhanced photocurrent properties also indicated that $C_{60}$ was encapsulated in the PIZA-1 thin film. This introduction of $C_{60}$ could increase the separation efficiency of photogenerated electrons and holes, resulting in the improved photoactivity. Besides, embedding $C_{60}$ in the PIZA-1 thin film increases the electrical conductivity compared with the PIZA-1 thin film (Fig. S14†). In addition, the stability of the $C_{60}$@PIZA-1 thin film was verified by XRD, IR and SEM. The XRD data (Fig. S15†) of the $C_{60}$@PIZA-1 thin film reveal that the diffraction pattern did not change before and after loading. Moreover, the IR spectra (Fig. S16†) and SEM images (Fig. S17†) of the $C_{60}$ loaded PIZA-1 thin film was similar to those of the pristine thin film. The IR spectral bands in the range of 1390–1700 $cm^{-1}$ corresponded to the vibrational stretching of carboxylate groups and pyrrole groups. Because the IR bands of $C_{60}$ overlapped with the PIZA-1 IR spectrum, the $C_{60}$@PIZA-1 spectrum didn't show the peak of $C_{60}$.

For comparison, the samples were adjusted to maintain an identical linear transmittance of ~85% at 532 nm. Fig. S18† shows the open-aperture Z-scan curves of the $C_{60}$@PIZA-1 thin film which exhibit a distinct reduction in transmittance when it reached the laser focus. The normalized transmittance gradually increased with the increasing incident pulse energy, indicative of the excellent optical limiting effect. The comparison results at the same incident pulse energy of 100 μJ are shown in Fig. 4a and S19.† The $C_{60}$@PIZA-1 thin film has the smallest transmittance of ~0.54 at the laser focus compared with the PIZA-1 thin film, $C_{60}$, porphyrin ligand and porphyrin ligand mixed with the $C_{60}$ film on quartz glass. The thicknesses of the compared films were about 200–250 nm as shown in Fig. S20.† This is because the presented PIZA-1 thin films have some

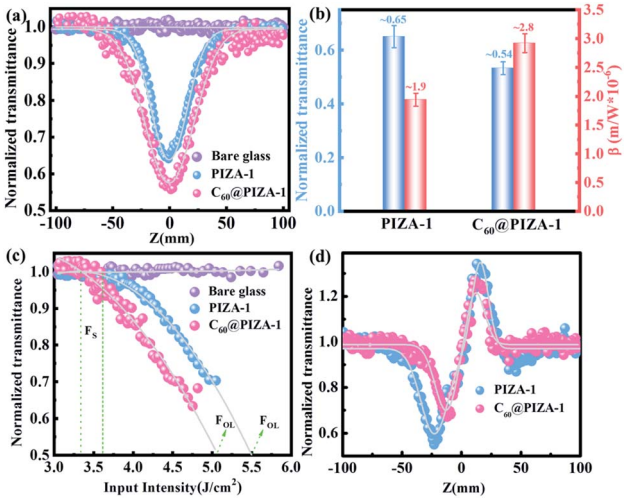


Fig. 4 (a) The open aperture plots and (b) comparison of nonlinear transmittance and nonlinear absorption coefficients ($\beta$) of the PIZA-1 and $C_{60}$@PIZA-1 thin films at 100 μJ; (c) variation in the normalized transmittance as a function of input intensity and (d) nonlinear refraction response of the PIZA-1 and $C_{60}$@PIZA-1 thin films at 100 μJ.

advantages, such as good orientation, low surface roughness and low laser scattering. Moreover, the curves of output fluence *versus* input fluence of the PIZA-1 and $C_{60}$@PIZA-1 thin films showed that the output fluence linearly increased at low-incident fluence as shown in Fig. S21.† However, at high-incident fluence, the output fluence deviated from linearity which is the typical behavior of the optical limiting response. To quantitatively evaluate the NLO responses of the samples, the measured Z-scan curves in Fig. 4a were fitted using eqn (1)–(3) in the experimental section.[48] By fitting the curves, the values of $\beta$ were obtained. The calculated $\beta$ values for the $C_{60}$@PIZA-1 thin film and PIZA-1 thin film are $\sim 2.8 \times 10^{-6}$ m $W^{-1}$ ($\sigma = 9 \times 10^{-8}$) and $\sim 1.9 \times 10^{-6}$ m $W^{-1}$ ($\sigma = 8 \times 10^{-8}$), respectively (Fig. 4b), indicating that the optical limiting effect of the PIZA-1 thin film can be improved by loading $C_{60}$. Furthermore, the optical limiting starting threshold ($F_S$) and optical limiting threshold ($F_{OL}$)[49] were evaluated to be 3.33 J $cm^{-2}$ and 5.04 J $cm^{-2}$ and 3.61 J $cm^{-2}$ and 5.51 J $cm^{-2}$ for the $C_{60}$@PIZA-1 and PIZA-1 thin films, respectively (Fig. 4c). The input fluence where the transmittance starts to decrease is called the optical limiting starting threshold ($F_S$) and the input fluence at which the transmittance decreases to half the linear transmittance is known as the optical limiting threshold (FOL). The lower $F_S$ and $F_{OL}$ exhibiting $C_{60}$@PIZA-1 thin film will be an ideal candidate for optical limiting applications. Similarly, the $C_{60}$@PIZA-1 thin film also showed a valley/peak signal (Fig. 4d) in the closed-aperture Z-scan data, indicating the self-focusing behavior of propagating light. The nonlinear refractive coefficients $\gamma$ for the PIZA-1 and $C_{60}$@PIZA-1 thin films were found to be $\sim 4.1 \times 10^{-13}$ $m^2$ $W^{-1}$ ($\sigma = 1.9 \times 10^{-14}$) and $\sim 3.5 \times 10^{-13}$ $m^2$ $W^{-1}$ ($\sigma = 1.5 \times 10^{-14}$) by fitting the curves in Fig. 4d. Using eqn (6)–(8), the nonlinear susceptibilities $\chi^{(3)}$ of the PIZA-1 and $C_{60}$@PIZA-1 thin films were calculated to be $\sim 7.7 \times 10^{-8}$ esu and $\sim 1.1 \times 10^{-7}$ esu, respectively. These results showed that $C_{60}$@PIZA-1 possesses better third-order optical nonlinearities than the PIZA-1 thin film.

Fullerenes ($C_{60}$), as a class of carbon-only molecules, have been considered favorable electron acceptors, while porphyrin serves as an electron donor. The observed luminescence quenching (Fig. S22†) indicates that there is a strong interaction between the excited state of PIZA-1 and the fullerene moieties in the $C_{60}$@PIZA-1 thin film. Possible pathways for the fluorescence quenching of the $C_{60}$@PIZA-1 thin film may be attributed to two possible competitive processes: photoinduced electron transfer (PET) and energy transfer (ET). An efficient ET/PET process in several porphyrin–carbon structure systems has been reported.[50–53] The photoinduced electron transfer can be evidenced by the photocurrent responses and the electrochemical impedance spectroscopy (EIS) measurements (Fig. S13 and S23†). Regarding the donor–acceptor structure and fluorescence quenching behavior, the ET/PET from the electron donor PIZA-1 to the acceptor fullerenes plays an important role in enhancing the optical limiting effect. In addition, the RSA, NLS and NLR of porphyrin and $C_{60}$ should be responsible for the third-order NLO response of the $C_{60}$@PIZA-1 thin film. Thanks to the accumulation effect of the RSA, NLS, NLR and ET/PET process, the $C_{60}$@PIZA-1 thin film exhibited superior NLO performance compared to the individual components.

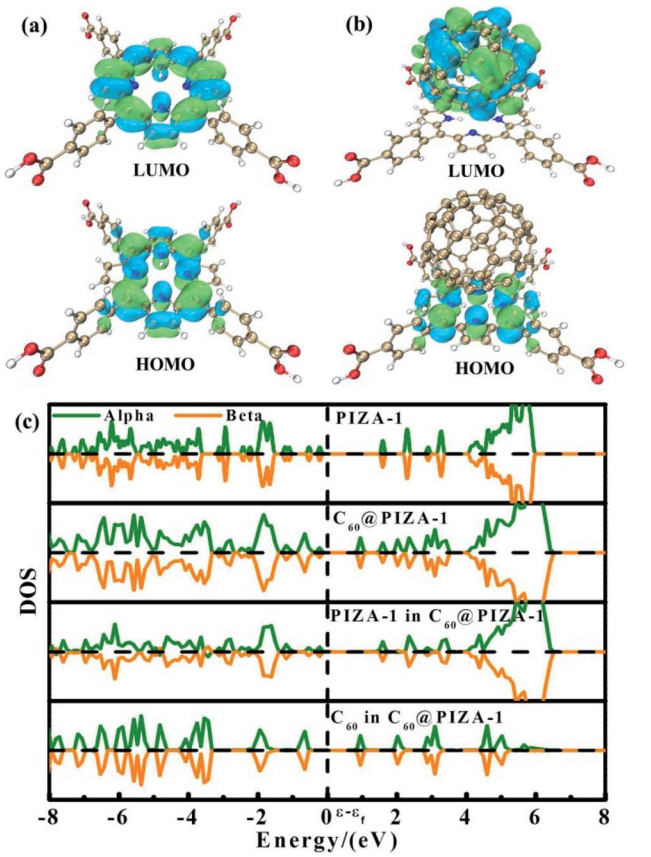


Fig. 5 The optimized structures of the PIZA-1 thin film (a) and $C_{60}$@PIZA-1 thin film (b); the corresponding density of states (DOS) calculations (c).

To gain further insight into the observed electron-donor/electron-acceptor interactions in the $C_{60}$@PIZA-1 thin film, theoretical calculations are carried out based on density functional theory (DFT). The optimized periodic structures and the results of electronic density of states (DOS) calculations for the PIZA-1 and $C_{60}$@PIZA-1 thin films are shown in Fig. 5. Compared with the PIZA-1, the valence band maximum (VBM) of the $C_{60}$@PIZA-1 is contributed by the PIZA-1, while the conduction band minimum (CBM) originates from the $C_{60}$ moiety. Besides, the calculated nominal band gap of the $C_{60}$@PIZA-1 thin film decreases by 0.66 eV compared with that of the PIZA-1 thin film, indicating that excited electrons easily transfer from the porphyrin to the $C_{60}$ moiety in the presence of laser light. The band gap of the $C_{60}$@PIZA-1 thin film was comparable or smaller than those of many reported porphyrin-fullerene systems (Table S2†). The occurrence of electron transfer herein is thought to be responsible for the enhancement of the third-order NLO properties. The combination of PIZA-1 with $C_{60}$ results in the improvement of the charge separation and transport capability between porphyrin groups and $C_{60}$ moieties, which is consistent with the results of photocurrent response and electrical conductivity. Resultantly, the structure of $C_{60}$@PIZA-1 with a high density of donor–acceptor interfaces had enhanced optical limiting responses.

# Conclusions

In summary, we have reported a layer by layer autoarm immersion method for preparing MOF thin films with a tunable thickness, homogeneous surface and effective guest loading. The third-order nonlinear absorption of PIZA-1 thin films was switched continuously between RSA and SA by tuning the thickness. Moreover, the optical limiting effect was improved by loading $C_{60}$ in the pores of the PIZA-1 thin film. The electronic DOS calculations demonstrated that the enhanced optical limiting effect of the $C_{60}$@PIZA-1 thin film was mainly attributed to the energy transfer/photoinduced electron transfer (ET/PET) between porphyrin groups and fullerenes. Taken as a whole, a promising thin film material for optical limiting is reported and it provides an insightful understanding of porphyrin-based MOF thin films for future broad optical applications in pulse compression, Q-switching, mode-locking and optical limiting.

# Experimental

### Materials and instrumentation

All of the chemicals purchased were used without further purification. The quartz glass and Si substrate were first cleaned using distilled water in an ultrasonic bath and dried before activation. And then they were treated with a mixture of a 0.2 mM NaOH aqueous solution and hydrogen peroxide (30%) with a volume ratio of 3 : 1 at 80 °C for 30 min and then cleaned with deionized water and dried under nitrogen flux for the next step. Powder X-ray diffraction (PXRD) analysis was performed on a MiniFlex2 X-ray diffractometer using Cu-K$\alpha$ radiation ($\lambda$ = 0.1542 nm) in the $2\theta$ range of 5–30° with a scanning rate of 0.5° $min^{-1}$. IRRAS data were recorded using a Bruker Vertex 70 FTIR spectrometer with 2 $cm^{-1}$ resolution at an angle of incidence of 80° relative to the surface normal. Scanning electron microscope (SEM) images showing the morphology of thin films were obtained using a JSM6700. AFM images were recorded with a Bruker Dimension ICON. The thickness was measured using a stylus profiler (Bruker DEKTAK XT). The UV-vis spectra of the samples were measured using a Lambda 365. Photoluminescence spectra were measured by using an Edinburgh Instruments FLS920. The photocurrent response was analyzed using a CHI760e electrochemical workstation (Shanghai Chenhua Instrument China).

### Fabrication of PIZA-1 thin films with different thicknesses

The PIZA-1 thin films used in the present work were grown using the layer-by-layer autoarm immersion method and were fabricated using the following diluted ethanolic solutions at room temperature: cobalt acetate (1.0 mM) and TCPP (5,10,15,20-(4-carboxyphenyl)porphyrin, 0.1 mM). The details are as follows: first, functionalized quartz glass was immersed in a solution of cobalt acetate for 10 min and then was immersed in a solution of TCPP for 15 min. After each step the glass was washed with pure ethanol to remove residual reactants. The above details represent one cycle. A total of 5, 10, 15, 20, and 25 growth cycles were used for PIZA-1 thin films grown on quartz glass.

### Fabrication of $C_{60}$ loaded PIZA-1 thin films

The $C_{60}$@PIZA-1 thin film was fabricated by the layer-by-layer autoarm immersion method. The substrate was immersed in cobalt acetate (1.0 mM), TCPP (5,10,15,20-(4-carboxyphenyl) porphyrin, 0.1 mM) and $C_{60}$ (0.2 mM) solutions sequentially. The immersion times were 10, 15, and 5 min for the $Co(OAc)_2$, TCPP ethanol solution and $C_{60}$ toluene solution, respectively. After each step the film was washed with pure ethanol to remove residual reactants. A total of 10 growth cycles were used for $C_{60}$ encapsulation in the PIZA-1 thin film in this work.

### Fabrication of the HKUST-1 thin film, MOF-2 thin film and $Co_2(BDC)_2TED$ thin film

The method of preparing the HKUST-1 thin film and MOF-2 thin film was the same as the fabrication method of the PIZA-1 thin film, except for the type of metal and linker solution. For the HKUST-1 thin film, the metal and linker solutions were copper acetate (1 mM) and BTC (1,3,5-benzenetricarboxylic acid, 0.4 mM), respectively. The metal and linker solutions were copper acetate (1 mM) and $H_2BDC$ (1,4-benzenedicarboxylic acid, 0.4 mM) for the MOF-2 thin film. The $Co_2(BDC)_2TED$ thin film was prepared at 50 °C. The metal and linker solutions were cobalt acetate (1 mM) and a mixed solution of $H_2BDC$ (1,4-benzenedicarboxylic acid, 0.4 mM) and TED (triethylenediamine, 0.4 mM), respectively.

### Fabrication of the porphyrin ligand, the $C_{60}$ and the porphyrin ligand mixed with $C_{60}$ films on quartz glass

A 0.1 mM TCPP (5,10,15,20-(4-carboxyphenyl)porphyrin) ethanol solution was coated on quartz glass using a drop-

coating method. After the solvent evaporated at room temperature, the TCPP ethanol solution was coated on quartz glass again. The above operation was repeated several times until the samples were adjusted to maintain an identical linear transmittance of ~85%. The preparation methods of the $C_{60}$ and the porphyrin ligand mixed with $C_{60}$ films on quartz glass were similar to the fabrication method of the porphyrin ligand film on quartz glass.

### Electrochemical measurements

The photocurrent tests and EIS were carried out on a CHI760e electrochemical workstation (Shanghai Chenhua Instrument China) in the three electrode electrochemical mode in a 0.2 M $Na_2SO_4$ aqueous solution at room temperature where a Pt wire served as the counter electrode and Ag/AgCl as the reference electrode; the PIZA-1 thin film and $C_{60}$@PIZA-1 thin film grown on FTO were directly used as the working electrode without any ancillary materials (electrode size of 1 × 1 $cm^2$). The photocurrent responses of the samples were recorded with a voltage bias of 0 V and the working electrode was illuminated using a 300 W Xe lamp (Beijing Perfect Light, PLS-SXE300C). The EIS measurements were carried out an open-circuit voltage in the frequency range from 0.1 Hz to 100 kHz with an amplitude of 5 mV and the working electrode was illuminated with a 532 nm laser.

### Quartz crystal microbalance (QCM) measurements

A commercial QCM 200 with a flow module for measurements in the gas phase was used to monitor the mass uptake and absorption rate of the synthesized PIZA-1 thin film and $C_{60}$@PIZA-1 thin film using 10 cycles, which were prepared on MUD SAM functionalized QCM working electrodes. The QCM can be used in gas phase environments for monitoring the change of mass by monitoring the resonance frequency changes on the electrode thin film. In this work, water was chosen as the loading analyte.

### Z-scan measurements

The nonlinear optical properties of the sample were evaluated using the Z-scan technique. The excitation light source was an Nd:YAG laser with a repetition rate of 10 Hz. The laser pulses (period, 5 ns; wavelength, 532 nm) were split into two beams with a mirror. The pulse energies at the front and back of the samples were monitored using energy detectors 1 and 2. All of the measurements were conducted at room temperature. The sample was mounted on a computer-controlled translation stage that shifted each sample along the *z*-axis.

The measured Z-scan curves were fitted using the following expressions:

$$T(Z, S=1) = \frac{1}{\sqrt{\pi}(Z,0)} \int_{-\infty}^{\infty} \mathrm{Ln}\left[1 + q_0(Z,0)\mathrm{e}^{-r^2}\right]\mathrm{d}r \quad (1)$$

$$q_0(Z,0) = \beta I_0 L_{\mathrm{eff}} \quad (2)$$

$$L_{\mathrm{eff}} = \frac{1-\mathrm{e}^{-\alpha l}}{\alpha} \quad (3)$$

$$T(Z,\Delta\Phi) = 1 + \frac{4\Delta\Phi x}{(x^2+9)(x^2+1)} \quad (4)$$

$$\Delta\Phi = 2\pi\gamma I_0 L_{\mathrm{eff}}/\lambda \quad (5)$$

$$\chi_{\mathrm{I}}^{(3)} = \frac{2\varepsilon_0 c^2 {n_0}^2}{3\omega}\beta \quad (6)$$

$$\chi_{\mathrm{R}}^{(3)} = \frac{4c{n_0}^2\varepsilon_0}{3} n_2 \quad (7)$$

$$|\chi^{(3)}| = \sqrt{\left(\chi_{\mathrm{R}}^{(3)}\right)^2 + \left(\chi_{\mathrm{I}}^{(3)}\right)^2} \quad (8)$$

In these equations, $I_0$ is the on-axis peak intensity at the focus ($Z = 0$), $L_{\mathrm{eff}}$ is the effective thickness of the sample, $\alpha_0$ is the linear absorption coefficient, $l$ is the sample thickness, $x = z/z_0$, $z$ is the Z-scan displacement, $\Delta\Phi$ is the phase change, $\varepsilon_0$ is the permittivity of vacuum, $c$ is the speed of light, $n_0$ is the refractive index of the medium, $\omega = 2\pi c/\lambda$, and $n_2(\mathrm{esu}) = \frac{cn_0}{40\pi}\gamma(\mathrm{m}^2\ \mathrm{W}^{-1})$. By fitting the curves, the nonlinear absorption coefficient $\beta$, the nonlinear refractive coefficient $\gamma$ and the third-order nonlinear susceptibilities $\chi^{(3)}$ were obtained.

## Conflicts of interest

There are no conflicts to declare.

## Acknowledgements

This work was supported by the Strategic Priority Research Program of the Chinese Academy of Sciences (XDB20000000), National Key Research and Development Program of China (2018YFA0208600), National Natural Science Foundation of China (21872148, 21935010 and 21601189) and Youth Innovation Promotion Association of Chinese Academy of Sciences (2018339). The authors thank Dr Mei Qiu for the theoretical calculations.

## Note and references

1 X. Tian, R. Wei, Q. Guo, Y. J. Zhao and J. Qiu, *Adv. Mater.*, 2018, **30**, 1801638.
2 J. M. Hales, J. Matichak, S. Barlow, S. Ohira, K. Yesudas, J.-L. Bredas, J. W. Perry and S. R. Marder, *Science*, 2010, **327**, 1485–1488.
3 S. Mukhopadhyay, C. Risko, S. R. Marder and J.-L. Brédas, *Chem. Sci.*, 2012, **3**, 3103–3112.
4 X. Liu, Q. Guo and J. Qiu, *Adv. Mater.*, 2017, **29**, 1605886.
5 Q. Guo, Y. Yao, Z. C. Luo, Z. Qin, G. Xie, M. Liu, J. Kang, S. Zhang, G. Bi, X. Liu and J. Qiu, *ACS Nano*, 2016, **10**, 9463–9469.

 

6 H. Rath, J. Sankar, V. PrabhuRaja, T. K. Chandrashekar, A. Nag and D. Goswami, *J. Am. Chem. Soc.*, 2005, **127**, 11608–11609.
7 X. Hou, J. Sun, Z. Liu, C. Yan, W. Song, H. L. Zhang, S. Zhou and X. Shao, *Chem. Commun.*, 2018, **54**, 10981–10984.
8 K. Liang, H. G. Zheng, Y. L. Song, M. E. Lappert, Y. Z. Li, X. Q. Xin, Z. X. Huang, J. T. Chen and S. F. Lu, *Angew. Chem., Int. Ed.*, 2004, **43**, 5776–5779.
9 D. M. A. S. Dissanayake, M. P. Cifuentes and M. G. Humphrey, *Coord. Chem. Rev.*, 2018, **375**, 489–513.
10 Y. Xu, W. Wang, Y. Ge, H. Guo, X. Zhang, S. Chen, Y. Deng, Z. Lu and H. Zhang, *Adv. Funct. Mater.*, 2017, **27**, 1702437.
11 Q. F. Chen, X. Zhao, Q. Liu, J. D. Jia, X. T. Qiu, Y. L. Song, D. J. Young, W. H. Zhang and J. P. Lang, *Inorg. Chem.*, 2017, **56**, 5669–5679.
12 L.-F. Chen and Q. Xu, *Science*, 2017, **358**, 304–305.
13 H. Wang, P. Rassu, X. Wang, H. W. Li, X. R. Wang, X. Q. Wang, X. Feng, A. X. Yin, P. F. Li, X. Jin, S. L. Chen, X. J. Ma and B. Wang, *Angew. Chem., Int. Ed.*, 2018, **57**, 16416–16420.
14 S. W. Li, Y. Dong, J. W. Zhou, Y. Liu, J. M. Wang, X. Gao, Y. Z. Han, P. F. Qi and B. Wang, *Energy Environ. Sci.*, 2018, **11**, 1318–1325.
15 S. S. Wang, L. Jiao, Y. Y. Qian, W. C. Hu, G. Y. Xu, C. Wang and H. L. Jiang, *Angew. Chem., Int. Ed.*, 2019, **58**, 10713–10717.
16 R. Medishetty, J. K. Zareba, D. Mayer, M. Samoc and R. A. Fischer, *Chem. Soc. Rev.*, 2017, **46**, 4976–5004.
17 R. Medishetty, V. Nalla, L. Nemec, S. Henke, D. Mayer, H. Sun, K. Reuter and R. A. Fischer, *Adv. Mater.*, 2017, **29**, 1605637.
18 R. Medishetty, L. Nemec, V. Nalla, S. Henke, M. Samoc, K. Reuter and R. A. Fischer, *Angew. Chem., Int. Ed.*, 2017, **56**, 14743–14748.
19 Y. J. Cui, R. J. Song, J. C. Yu, M. Liu, Z. Q. Wang, C. D. Wu, Y. Yang, Z. Y. Wang, B. L. Chen and G. D. Qian, *Adv. Mater.*, 2015, **27**, 1420–1425.
20 Z. Wang, C. Y. Zhu, J. T. Mo, P. Y. Fu, Y. W. Zhao, S. Y. Yin, J. J. Jiang, M. Pan and C. Y. Su, *Angew. Chem., Int. Ed.*, 2019, **58**, 9752–9757.
21 J. Li, D. Jia, S. Meng, J. Zhang, M. P. Cifuentes, M. G. Humphrey and C. Zhang, *Chem.–Eur. J.*, 2015, **21**, 7914–7926.
22 X. Jiang, L. Zhang, S. Liu, Y. Zhang, Z. He, W. Li, F. Zhang, Y. Shi, W. Lü, Y. Li, Q. Wen, J. Li, J. Feng, S. Ruan, Y.-J. Zeng, X. Zhu, Y. Lu and H. Zhang, *Adv. Opt. Mater.*, 2018, **6**, 1800561.
23 R. J. Niu, W. F. Zhou, Y. Liu, J. Y. Yang, W. H. Zhang, J. P. Lang and D. J. Young, *Chem. Commun.*, 2019, **55**, 4873–4876.
24 K. Ikigaki, K. Okada, Y. Tokudome, T. Toyao, P. Falcaro, C. J. Doonan and M. Takahashi, *Angew. Chem., Int. Ed.*, 2019, **58**, 6886–6890.
25 P. Falcaro, K. Okada, T. Hara, K. Ikigaki, Y. Tokudome, A. W. Thornton, A. J. Hill, T. Williams, C. Doonan and M. Takahashi, *Nat. Mater.*, 2017, **16**, 342–350.
26 T. Haraguchi, K. Otsubo, O. Sokota, A. Fujiwara and H. Kitagawa, *J. Am. Chem. Soc.*, 2016, **138**, 16787–16793.
27 J. X. Liu and C. Woll, *Chem. Soc. Rev.*, 2017, **46**, 5730–5770.
28 S. L. Qiu, M. Xue and G. S. Zhu, *Chem. Soc. Rev.*, 2014, **43**, 6116–6140.
29 H. K. Arslan, O. Shekhah, J. Wohlgemuth, M. Franzreb, R. A. Fischer and C. Woell, *Adv. Funct. Mater.*, 2011, **21**, 4228–4231.
30 O. Shekhah, H. Wang, S. Kowarik, F. Schreiber, M. Paulus, M. Tolan, C. Sternemann, F. Evers, D. Zacher, R. A. Fischer and C. Woll, *J. Am. Chem. Soc.*, 2007, **129**, 15118–15119.
31 Z.-G. Gu and J. Zhang, *Coord. Chem. Rev.*, 2019, **378**, 513–532.
32 J. L. Zhuang, M. Kind, C. M. Grytz, F. Farr, M. Diefenbach, S. Tussupbayev, M. C. Holthausen and A. Terfort, *J. Am. Chem. Soc.*, 2015, **137**, 8237–8243.
33 L. Heinke and C. Woll, *Adv. Mater.*, 2019, **31**, 1806324.
34 W. J. Li, S. Watzele, H. A. El-Sayed, Y. C. Liang, G. Kieslich, A. S. Bandarenka, K. Rodewald, B. Rieger and R. A. Fischer, *J. Am. Chem. Soc.*, 2019, **141**, 5926–5933.
35 B. Liu, M. Tu, D. Zacher and R. A. Fischer, *Adv. Funct. Mater.*, 2013, **23**, 3790–3798.
36 Z.-G. Gu, H. Fu, T. Neumann, Z.-X. Xu, W.-Q. Fu, W. Wenzel, L. Zhang, J. Zhang and C. Woell, *ACS Nano*, 2016, **10**, 977–983.
37 X. Liu, M. Kozlowska, T. Okkali, D. Wagner, T. Higashino, G. Brenner-Weifss, S. M. Marschner, Z. Fu, Q. Zhang, H. Imahori, S. Braese, W. Wenzel, C. Woell and L. Heinke, *Angew. Chem., Int. Ed.*, 2019, **58**, 9590–9595.
38 D.-J. Li, Z.-G. Gu, W. Zhang, Y. Kang and J. Zhang, *J. Mater. Chem. A*, 2017, **5**, 20126–20130.
39 D. Feng, Z. Y. Gu, J. R. Li, H. L. Jiang, Z. Wei and H. C. Zhou, *Angew. Chem., Int. Ed.*, 2012, **51**, 10307–10310.
40 A. M. Shultz, O. K. Farha, J. T. Hupp and S. T. Nguyen, *J. Am. Chem. Soc.*, 2009, **131**, 4204–4205.
41 H. L. Jiang, D. W. Feng, K. C. Wang, Z. Y. Gu, Z. W. Wei, Y. P. Chen and H. C. Zhou, *J. Am. Chem. Soc.*, 2013, **135**, 13934–13938.
42 M. O. Senge, M. Fazekas, E. G. A. Notaras, W. J. Blau, M. Zawadzka, O. B. Locos and E. M. Ni Mhuircheartaigh, *Adv. Mater.*, 2007, **19**, 2737–2774.
43 S. U. Hassan, F. Nawaz, Z. U. Haq Khan, A. Firdous, M. A. Farid and M. S. Nazir, *Opt. Mater.*, 2018, **86**, 106–112.
44 D.-J. Li, Z.-G. Gu, I. Vohra, Y. Kang, Y.-S. Zhu and J. Zhang, *Small*, 2017, **13**, 1604035.
45 M. Shi, S. Huang, N. Dong, Z. Liu, F. Gan, J. Wang and Y. Chen, *Chem. Commun.*, 2018, **54**, 366–369.
46 Z.-B. Liu, Y.-F. Xu, X.-Y. Zhang, X.-L. Zhang, Y.-S. Chen and J.-G. Tian, *J. Phys. Chem. B*, 2009, **113**, 9681–9686.
47 B. P. Biswal, S. Valligatla, M. Wang, T. Banerjee, N. A. Saad, B. M. K. Mariserla, N. Chandrasekhar, D. Becker, M. Addicoat, I. Senkovska, R. Berger, D. N. Rao, S. Kaskel and X. Feng, *Angew. Chem., Int. Ed.*, 2019, **58**, 6896–6900.
48 Z.-G. Gu, D.-J. Li, C. Zheng, Y. Kang, C. Wöll and J. Zhang, *Angew. Chem., Int. Ed.*, 2017, **56**, 6853–6858.
49 G. Liang, L. Tao, Y. H. Tsang, L. Zeng, X. Liu, J. Li, J. Qu and Q. Wen, *J. Mater. Chem. C*, 2019, **7**, 495–502.

50 Y. Xu, Z. Liu, X. Zhang, Y. Wang, J. Tian, Y. Huang, Y. Ma, X. Zhang and Y. Chen, *Adv. Mater.*, 2009, **21**, 1275–1279.
51 H. Xu, P. Wu, C. Liao, C. Lv and Z. Gu, *Chem. Commun.*, 2014, **50**, 8951–8954.
52 A. Wang, J. Ye, M. G. Humphrey and C. Zhang, *Adv. Mater.*, 2018, **30**, 1705704.
53 N. Karousis, A. S. D. Sandanayaka, T. Hasobe, S. P. Economopoulos, E. Sarantopoulou and N. Tagmatarchis, *J. Mater. Chem.*, 2011, **21**, 109–117.